Relationships Among SST Variability, Physical, and Biological Parameters in the Northeastern Indian Ocean

Thushani Suleka Madhubhashini Elepathage [1,2,3,*] and Danling Tang [1,2,*]

[1] Guandong Key Laboratory of Ocean Remote Sensing, South China Sea Institute of Oceanology, Chinese Academy of Sciences, Guangzhou, People's Republic of China
[2] College of Earth and Planetary Sciences, University of Chinese Academy of Sciences, Beijing 100049, People's Republic of China
[3] Department of Animal Science, Faculty of Agriculture, University of Peradeniya, Peradeniya, Sri Lanka

[Original manuscript received 24 April 2019; accepted 16 April 2020]

ABSTRACT *This study modelled physical and biological changes in the Bay of Bengal, the Arabian Sea, and the exclusive economic zone around Sri Lanka by examining the relationships between sea surface temperature (SST) and a range of biological and physical variables allowing prediction of the changes in the variables studied with changing temperature. Datasets were extracted from satellite data from 2003 to 2015. Boosted regression trees (BRT) were used to model the data and identify their (non-linear) relationships. Within the study region and based on the BRT model, nitrate, latent heat flux, wind speed, and chlorophyll* a *(chl* a*) concentration in open water were found to have negative relationships with SST, while air temperature and ozone mass mixing ratio had positive relationships. Seasonal peak values of wind speed and chl* a *concentrations occurred from June to August. Peak SST and air temperature values occurred from March to May, peak nitrate and latent heat values from September to November, and peak ozone mass mixing ratios from December to February. The highly correlated ranges of air temperature, nitrate concentration, open water latent energy flux, surface wind speed, chl* a *concentration, and ozone mass mixing ratio for SST above 28°C were 299–300.5 K, >0.2 µmol* L^{-1}*, 120–160 W* m^{-2}*, 4–8 m* s^{-1}*, 0.1–1 mg* m^{-3}*, and 4.5–5.5 ×* 10^{-8}*, respectively.*

RÉSUMÉ *[Traduit par la rédaction] Dans cette étude, nous modélisons des paramètres physiques et biologiques dans le golfe du Bengale, la mer d'Oman et la zone économique exclusive qui borde le Sri Lanka, en examinant la relation entre la température de surface de la mer (SST) et une série de variables biologiques et physiques, afin de prévoir les variations des paramètres étudiés en fonction de l'évolution de la température. Nous avons extrait des ensembles de données (2003 à 2015) à partir de données satellitaires. Nous nous sommes servi d'arbres de régression renforcés afin de modéliser les données et de déterminer leurs relations (non linéaires). Dans la région étudiée, et sur la base du modèle de régression, nous constatons que la concentration de nitrate, le flux de chaleur latente, la vitesse du vent et la concentration de chlorophylle* a *(chl* a*) en eau libre montrent une relation inverse avec la SST, tandis que la température de l'air et le rapport de mélange de l'ozone varient directement. Les valeurs maximales saisonnières de la vitesse du vent et des concentrations de chl* a *se produisent de juin à août. Les valeurs maximales de la SST et de la température de l'air se produisent de mars à mai; les valeurs maximales du nitrate et de la chaleur latente, de septembre à novembre; et les rapports de mélange maximaux de l'ozone, de décembre à février. Les intervalles de valeurs fortement corrélés de la température de l'air, de la concentration de nitrate, du flux d'énergie latente en eau libre, de la vitesse du vent en surface, de la concentration de chl* a *et du rapport de mélange de l'ozone pour une SST supérieure à 28°C étaient respectivement 299 à 300,5 K; >0.2 µmol* L^{-1}*; 120 à 160 W* m^{-2}*; 4 à 8 m* s^{-1}*; 0,1 à 1 mg* m^{-3} *et 4.5 à 5.5 ×* 10^{-8}*.*

1 Introduction

Many parts of the Indian Ocean, including the Bay of Bengal (BoB), Arabian Sea (AS), and the exclusive economic zone of Sri Lanka, are considered highly productive areas because of a variety of physical and chemical processes that are affected by seasonal monsoonal changes (De Vos et al., 2014; Kay et al., 2018; Qasim, 1982). Thus, the monsoon seasons in this region play an integral role in the spatial variability of several environmental parameters in the North Indian Ocean (NIO) including surface winds, currents, salinity, and sea surface temperature (SST) (D'Addezio et al., 2015). The rain that occurs with monsoonal variability is a major factor affecting

*Corresponding authors' emails: thushani@scsio.ac.cn, ~~lingzistdlw126.com~~

agriculture within this region (O. B. Kumar et al., 2004). Moreover, SST and phytoplankton productivity in this region governs fish distribution, which is important not only for fisheries but also for ecosystem balance (P. S. Kumar et al., 2014; Madhubhashini et al., 2019; Yapa, 2009).

One of the major factors regulating oceanic ecosystems is SST (Sarmiento et al., 1999). The Indian Ocean has the second highest average SST among the global oceans (Hansen et al., 1997). Recently, anthropogenic activities have driven rapid changes in the marine ecosystems of the eastern and western gulfs of the AS and the Red Sea including coral bleaching and the destruction of seagrass habitats (Govil & Naidu, 2011; Nandkeolyar et al., 2013). The Persian Gulf and Red Sea are also reported to be warming rapidly (Govil & Naidu, 2011; Nandkeolyar et al., 2013). The SST in the open ocean of the AS varies bimodally, with warming events occurring in the spring and fall inter-monsoon seasons and cooling events occurring in the southwest and northeast during the monsoon seasons (Govil & Naidu, 2011; Humaira et al., 2019; Khole, 2003). The SST is a difficult parameter to quantify; the upper 10 m of the open ocean has a complex and variable vertical temperature structure related to ocean turbulence and air–sea fluxes of heat, moisture, and momentum (Shamsad et al., 2013), which in turn regulate monsoonal variations and circulation patterns.

The NIO is affected by semi-annual wind-driven ocean circulation patterns (Kay et al., 2018; Qasim, 1982). Because both the AS and the BoB basins share the same latitudinal range, they are both affected by semi-annual reversing monsoonal winds (Lévy et al., 2007; Wiggert et al., 2005). During the boreal summer, winds blow from the southwest, and during the boreal winter winds are from the northeast. This wind-reversal phenomenon triggers a seasonal reversal in upper-ocean circulation patterns, stimulating changes in vertical mixing, upwelling, and downwelling patterns (Sarangi & Nanthini Devi, 2017). These changes in the physical environment induce blooms of a variety of phytoplankton (Lee et al., 2000; Murtugudde et al., 2007; Shankar et al., 2002).

In the AS, a regional climate shift has been observed since 1995, and the frequency of intense cyclones in the region has also increased (S. P. Kumar et al., 2009). These cyclones can trigger the upward cycling of nutrients into the euphotic zone (Sarangi & Nanthini Devi, 2017). In comparison, the BoB is a semi-enclosed basin, and its circulation patterns are rather complex. The major riverine systems in this region, such as the Ganges–Hooghly, Padma, Brahmaputra–Jamuna, Barak–Surma–Meghna, Irrawaddy, Godavari, Mahanadi, Brahmani, Baitarani, Krishna, and Kaveri, discharge a significant amount of fresh water into the BoB, creating a low-salinity system of less than 34 (Narvekar & Prasanna Kumar, 2014; Sarma et al., 2013).

The exchange of heat and moisture between the ocean and atmosphere in this region also affects monsoonal rainfall. However, in the NIO, the factors associated with variations in SST have not yet been identified. Hence, the interrelationships between atmospheric and oceanic variations in this region require further assessment to better understand and characterize this complex system (Roxy et al., 2013; Sengupta et al., 2007).

It is well known that the oceans play a major role in regulating global climate variability (Shukla, 1998); several aspects of climate change result from coupled air–sea interactions, such as the El Niño–Southern Oscillation (ENSO). Atmospheric general circulation model studies have shown that zonal-mean tropospheric temperature hikes result from SST increments in the Tropical Indian Ocean and the Atlantic Ocean (A. Kumar & Hoerling, 2003; Lau et al., 2005). One of the major factors affecting atmospheric and oceanic variability and predictability are SST anomalies (Shukla, 1998; Trenberth et al., 1998). Although large-scale variability and anomalies have been studied previously, changes specific to particular regions have seldom been considered. Thus, understanding of the physical and ecological dynamics related to SST in the NIO has not advanced in several regards because the region is under-sampled and less often studied than the Pacific and Atlantic Oceans. Furthermore, given that it is influenced by monsoonal cycles, the NIO is a dynamically complex and highly variable system (Sumesh & Ramesh Kumar, 2013). Indeed, many physical, biogeochemical, and ecological impacts of monsoons on this complex system have yet to be studied in detail (Hood et al., 2008).

This study examined the seasonal dynamics of a region within the NIO, such as SST variability and the changes in a number of potential predictor variables. This study also identified the effect of SST on biological parameters, such as phytoplankton density. Several physical parameters are interlinked and affect the physicochemical and biological changes in the NIO. For example, latent heat flux is primarily controlled by wind speed over the warm pool that develops in the AS (Izumo et al., 2008). The Somalia–Oman upwelling region is regulated by SST where the winds are strong (Izumo et al., 2008). Furthermore, latent heat flux changes in the NIO are principally triggered by SST changes (Izumo et al., 2008). Evaporation is also particularly affected by upwelling along the Somalia–Oman coasts; the ratio of latent heat flux to SST increases during periods of enhanced evaporation. In addition to physical parameters, many chemical parameters are also interlinked and regulate physicochemical and biological phenomena. Nitrogen, for example, is linked to the primary production rate, and nitrate can be supplied by diffusion across the thermocline (Sarangi, 2011). Studies suggest that SST, nitrate concentration, and primary productivity are interrelated (Kamykowski, 1987). However, the relationship between nitrate concentration and SST has not yet been extensively studied. Other chemical parameters include ozone concentration, which is affected by a combination of anthropogenic pollution and biomass burning modulated by air mass transport (Sonkaew & Macatangay, 2015). However, the linkages between ozone mixing ratios and changes in other physical parameters remain unstudied. Moreover, this study aimed to identify how SST and its associated variables affect biological components, such as chlorophyll *a* (chl *a*) concentrations in the NIO, specifically in the BoB, the AS, and the Sri Lankan exclusive economic zone. Because the relationships among the physical, chemical, and biological components of the ocean differ from one region to another, it is important to correctly identify their regional relationships. The results from this study can, therefore, provide important insights for policymakers, environmental conservationists, and disaster managers in predicting future environmental changes that may occur in the NIO. The SST governs the biological activity, ecological and biogeochemical processes, water metabolism, habitat characteristics, momentum, gas and heat exchange between the upper ocean layers and the atmosphere (Ding & Elmore, 2015; Karagali et al., 2012). Information about SST is extremely important for scientific, commercial, and social activities (Oke et al., 2015), such as weather forecasting, air–sea interaction modelling, climate change studies, fisheries, and coastal zone management (Karagali et al., 2012). This study will provide the necessary information for all these sectors in support of better decision making and management. Satellite remote sensing provides the opportunity to study these dynamic processes of oceans at regional, as well as global, scales (Tang & Pan, 2011). We utilized this opportunity to devise several new innovations with the help of geographic information systems and statistics.

2 Materials and methods

a *Study Area*

Sri Lanka is located within the equatorial belt of the NIO. This island experiences seasonally reversing monsoons (De Vos et al., 2014). Sri Lanka is positioned with the AS to the west and the BoB to the east. Offshore, water and nutrients are transported by reversing ocean currents driven by monsoon winds (De Vos et al., 2014). The NIO experiences reversing monsoon winds bi-annually. The southwest monsoon generally occurs between May and September, and the northeast monsoon occurs from December through to March (Department of Meteorology, 2018; Tomczak, 1988). The intermonsoon periods are from March to April and October to November (Department of Meteorology, 2018). The Southwest Monsoon Current flows from the AS (to the west) to the east, transporting higher-salinity water during the southwest monsoon period. During the northeast monsoon period, the currents reverse, with the Northeast Monsoon Current transporting lower-salinity water from the BoB (to the east) to the west (Schott et al., 1994). During the southwest monsoon period, when the winds blow parallel to the coast, conditions are favourable for Ekman pumping to occur (Vinayachandran et al., 2004).

Sri Lanka has a narrow (2.5–25 km, mean = 20 km), shallow (30–90 m), and steep continental shelf that is narrowest at the eastern and southern parts of the island and broadens to merge with the Indian continental shelf towards the north and northwest (Vinayachandran et al., 2004). The mean width of the continental shelf is less than 10 km along the southwestern coast of the island (Vinayachandran et al., 2004), is concave, and extends to between 100 and 4000 m depth (Vinayachandran et al., 2004). The abyssal plain is 3000–4000 m deep (Swan, 1983).

The BoB receives approximately 1500 km^3 yr^{-1} of freshwater through run-off, while the total freshwater input into the AS is approximately 190 km^3 yr^{-1} (Jensen, 2001). Because evaporation from the AS is higher relative to its freshwater input, salinity is high (averaging approximately 36.5). In comparison, there is a positive freshwater supply to the BoB and salinity is, therefore, lower (<33) (Jensen, 2001).

The specific study region is located within the area 0° to 22°N and 72° to 98.5°E and contains the BoB, the AS, and the Sri Lankan exclusive economic zone (Fig. 1). To improve the precision of the modelling, the area from 5° to 10°N and 76° to 85°E was considered in detail. Here, warming of the BoB and the AS drives cyclonic storms (Chakrabarthi, 2019) and extreme rainfall (Sharma, 2017) in the NIO, having serious impacts on nearby countries. Moreover, this region affects the dynamics of the Madden–Julian Oscillation and the Indian Ocean Dipole, thus having specific importance from a climatological point of view.

b *Satellite Data*

Atmospheric and oceanic data were obtained from satellite imagery collected between 2003 and 2015 (NASA, 2016). Data from the Modern Era-Retrospective Analysis for Research and Applications (MERRA)-2 satellite were used to extract surface wind speeds (metres per second), ozone mass mixing ratios, and open water latent energy fluxes (Watts per square metre) at a resolution of $0.5° \times 0.625°$. Atmospheric infrared sounder (AIRS) data were used to obtain air temperatures (Kelvin) at a resolution of 0.1°. Moderate Resolution Imaging Spectroradiometer (MODIS)–Aqua Level 3 data were used to extract SST (degrees Celsius) and chl *a* concentration (milligrams per cubic metre) at a resolution of 4 km^2. Assimilation data from the National Aeronautics and Space Administration (NASA) Ocean Biogeochemical Model (NOBM) were used to obtain nitrate concentrations (micromoles per litre) at a resolution of $0.67° \times 1.25°$. The quantification of the variability in environmental variables derived from sensors with different spatial resolutions was assessed by spatially degrading the satellite sensor's derived data products to coarser spatial resolutions than their respective native resolutions (Dorji & Fearns, 2017). The degradation of the spatial resolution depended on the respective sensor's native resolution; the MODIS–Aqua data were degraded to 2–4 km at 2 km intervals, and the MERRA-2, AIRS, and NOBM data were degraded to 110 km at 110–120 km intervals. The spatial resolution was degraded using the aggregate of all available pixel values in a selected region.

c *Data Analysis*

Recent studies have shown that boosted regression tree (BRT) models perform well in ecological variable change

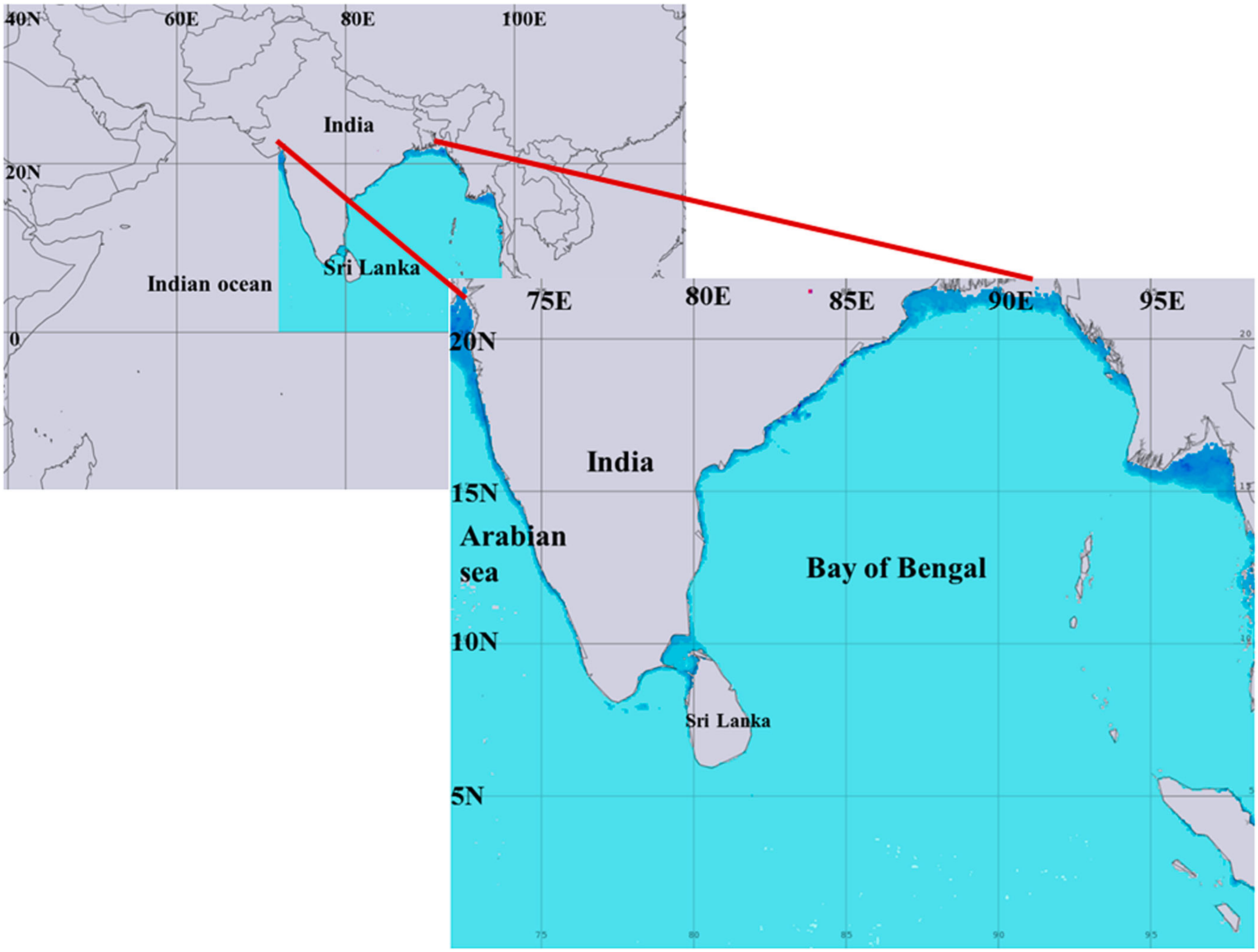

Fig. 1 The study area bounded by 0° to 22°N and 72° to 98.5°E. The study area is demarcated in blue and the land masks are in grey.

analyses (De'ath, 2007; Elith et al., 2008; Elith & Leathwick, 2017). The BRT modelling approach consists of a large set of relatively simple tree models that fit complex functions that describe the relationships between response variables and predictor variables (Elith et al., 2008). In the course of conducting this study, many variables were studied first using SST data; the number of trees fitted in each model round was increased gradually while using the residual deviance as a measure of model performance. A series of different BRT models were fitted to the data, depending on the response variable and spatial scale of interest. To simplify the resulting model, non-influential variables were also removed keeping only the significant variables ($p < 0.05$) fitted in the final model. The relative influence of the different explanatory variables was calculated based on the number of times a particular variable was selected for "splitting" during BRT construction and was averaged across all trees weighted by the squared improvement of the model fit (Elith et al., 2008). A five-fold cross-validation procedure (Shono, 2001) was used to assess and validate the predictive power of the models. The percentage of deviance explained and root mean square error of the different combinations of training and test sets from the cross-validation were the main criteria used in the final model selection. Deviance is used as the loss function. In logistic regression, the negative gradient of the deviance BRT model or a Poisson BRT model is the residual between the response and the fitted probability or fitted Poisson mean. These are fitted by a tree, and the fitted values are added to the current logit response or log (response).

3 Results

a *Monthly, Seasonal, and Interannual Variations*

According to the monthly variations of the studied variables (Fig. 2), SST had an increasing trend from January to April reaching a peak of 29.57°C. The SST showed a decline from April to July and increased again in September to 28.62°C. It reached 27.54°C again in December after the second decline. Air temperature had a maximum in May (27.89°C) after increasing from January, which had a minimum mean temperature of 25.45°C. The temperature

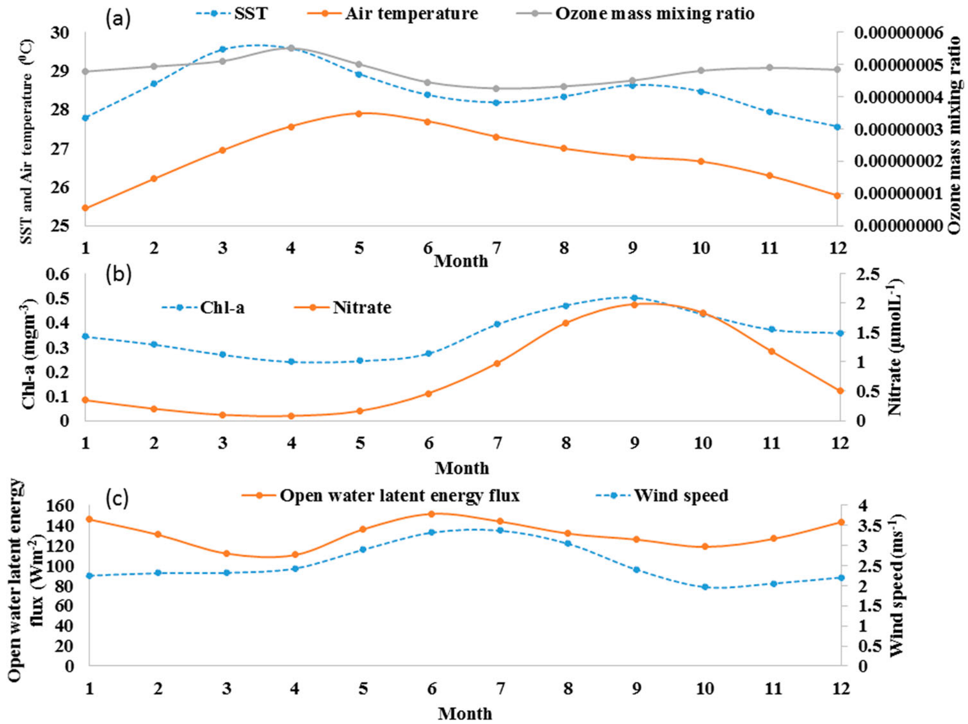

Fig. 2 Monthly mean changes of (a) SST, air temperature, and ozone mass mixing ration; (b) chl *a* and nitrate; and (c) open water latent energy flux and wind speed.

then decreased steadily from May till January. The concentration of chl *a* peaked in September at 0.5 mg m^{-3} after reaching a minimum of 0.24 mg m^{-3} in April when the SST was at its highest, so it is clear that the concentration of chl *a* increased from September to April. Nitrate also displayed the same pattern as chl *a*, reaching a peak in September (1.97 μmol L^{-1}) and a minimum in April (0.08 μmol L^{-1}). Wind speed peaked in July (3.37 m s^{-1}) and reached a minimum in October (1.96 m s^{-1}). Wind speed increased from October to July and decreased from July to October. Ozone mass mixing ratio had the highest peak in April (5.51×10^{-8}) and a second peak in November (4.89×10^{-8}). The minimum occurred in July (4.24×10^{-8}). The ozone mass mixing ratio increased from January to April and from July to November. The highest peak of open water latent energy flux occurred in June (151.5 W m^{-2}) and a secondary peak occurred in January (145.86 W m^{-2}). The lowest value was observed in April (110.48 W m^{-2}) and the second lowest in October (118.55 W m^{-2}).

Among the variables addressed, SST and air temperature increased by 0.0197°C per month and 0.0002 K per month, respectively (Fig. 3). The 2003, 2007, 2012, and 2015 maps in Fig. 3 show that, between March and May, chl *a* concentration decreased, SST increased, and air temperature increased. When the seasonal plots of the variables studied (Fig. 4) were analyzed, sea surface temperature (Fig. 4a) showed an increasing trend during all seasons. Within the study region, SST reached 29.47°C in the March to May season in 2010. This is the season for peak SST. The highest mean air temperature (Fig. 4b) also occurred during the March to May season and the lowest temperature occurred during the December to February season. The highest mean air temperature within the study area occurred in 2006 (28.6°C or 301.813 K) during the same season. Mean chl *a* (Fig. 4c), as well as wind speed, reached a peak during June, July, and August and a minimum in the March to May season. Nitrate concentration (Fig. 4d) had considerable increases and decreases within the study period especially in the September to November and June to August seasons. Nitrate concentrations in the September to November season are comparatively higher than in other seasons. Nitrate concentrations during the September to November season were particularly low in 2004, 2006, 2008, and 2011. The values were comparatively higher in 2003, 2005, 2007, 2009, and 2010. The highest value was observed during the September to November season in 2003 (8.58 μmol L^{-1}). Nitrate concentrations in September to November and June to August decreased from 2003 to 2015. The lowest nitrate concentrations occurred during the March to May season within the study period. The highest chl *a* concentration was observed in the June to August season of 2010 (1.61 mg m^{-3}), and the highest wind speed (Fig. 4e) in 2004 (8.97 m s^{-1}) in the same season. In most of the years, the ozone mass mixing ratio (Fig. 4f) was high during the March to May season and lowest during the June to August season. However, in 2003 and 2004 the ratio was higher in the December to February season than in March to May season. Hence, the highest value of the ozone mass mixing ratio was observed in 2004 in the December to February season (5.30×10^{-8}). Open water latent energy fluxes in the December to February and June to August

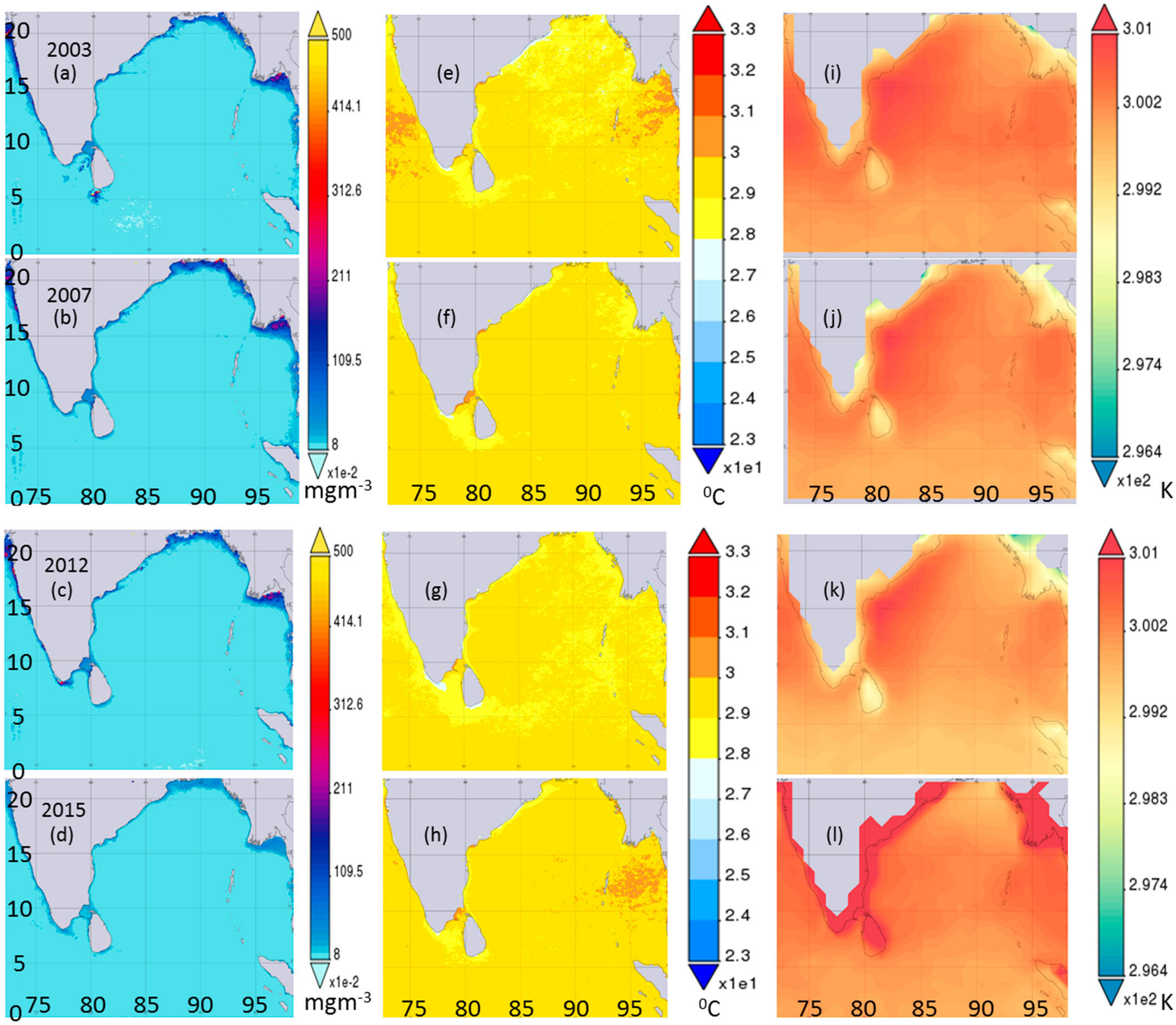

Fig. 3 The changes in (a)–(d) chl *a* concentrations, (e)–(h) SST, and (i)–(l) air temperature. The year for the changes is given on the first panel of each row.

seasons (Fig. 4g) were comparatively higher than in other seasons. In 2003, 2004, 2006, 2008, 2011, 2012, and 2015 latent energy flux was higher in the June to August season than in the December to February season.

b *Boosted Regression Tree Models*

The BRT models performed satisfactorily (achieving a training correlation of 0.999) at explaining variations in SST within the study region (Table 1). The models were developed using five-fold cross-validation, with a reasonable starting point to run the model defined by a tree complexity of 5, a learning rate of 0.01, and a bag.fraction of 0.5. When the model complexity increases, variance increases decreasing the bias (De'ath, 2007). Prediction error initially improves when the complexity increases. However, it typically reaches a minimum before increasing (Fig. 5). Figure 6 shows the change in holdout deviance with respect to the increment of number of trees. After each fold is processed, the average holdout residual deviance, standard error, and the optimum number of trees were calculated for the particular function as that at which the holdout deviance is minimized. The performance of each model was assessed by correlating the observed and predicted values and the percentage of total variance explained. All predictors contributed some level of relative influence; however, the predictors that had a relative influence of less than 2% were not included in the simplified model. The relative influences of the predictors used in the simplified BRT model are listed in Table 2. Of the six variables included in the simplified model, air temperature explained the largest proportion of SST variability (47.1%),

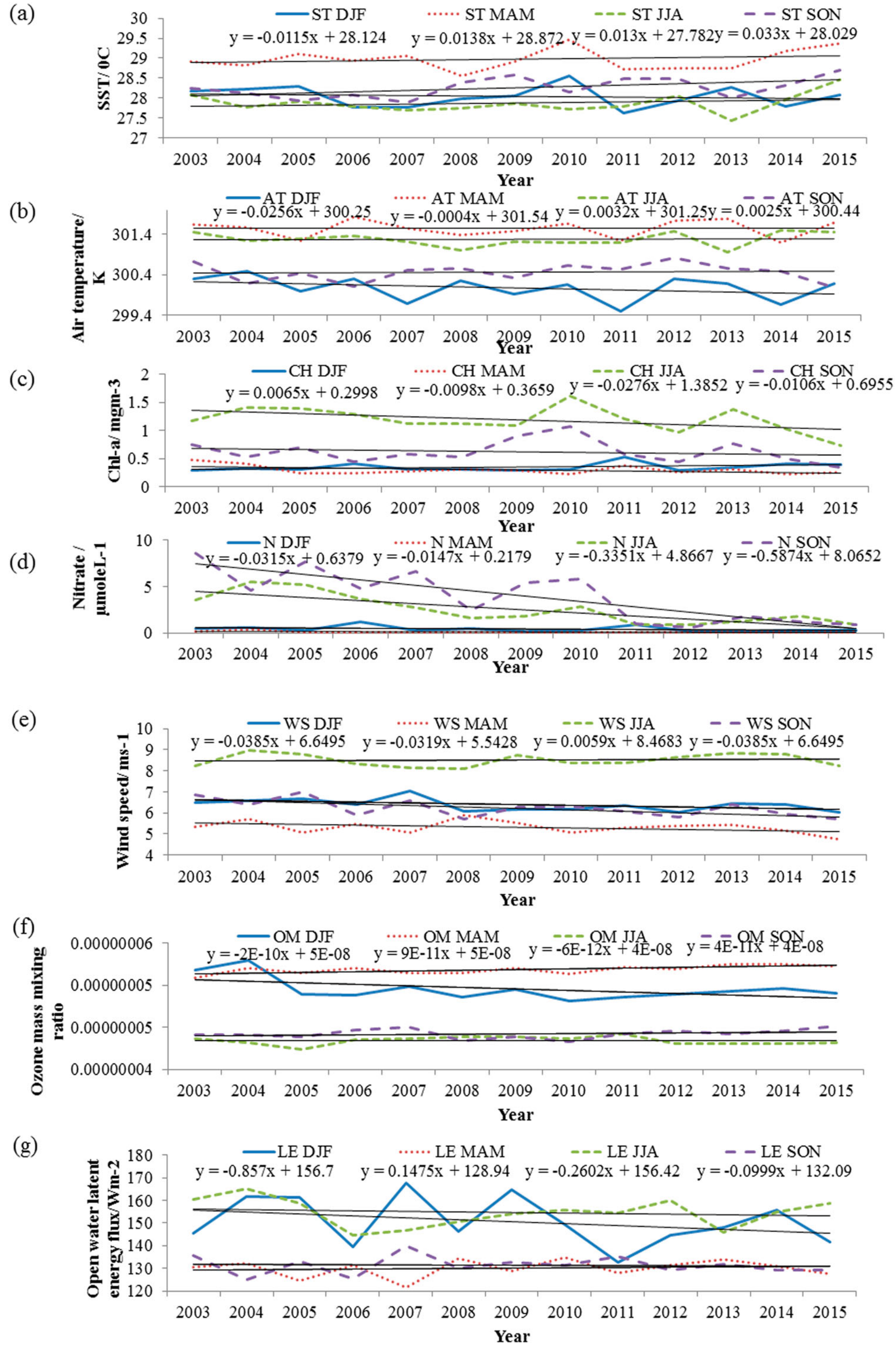

Fig. 4 Seasonal plots of environmental variables within the study region (a) SST; (b) air temperature; (c) chl *a* concentration; (d) nitrate concentration; (e) wind speed; (f) ozone mass mixing ratio; and (g) open water latent energy flux.

TABLE 1. Cross-validation performance assessment of the BRT models based on the correlation (CV) across folds.

	Base Model	Simplified Model
Number of predictors	44	7
Training Correlation	1	0.999
% Total variance	41	41.3
CV correlation	0.935	0.932

followed by nitrate concentration (17.6%), open water latent energy flux (5.5%), surface wind speed (4.8%), chl *a* concentration (2.6%), and ozone mass mixing ratio (2.2%) (Table 2).

The temporal relationships between variations in SST and the predictor variables were complex (Fig. 7). Figures 7 and 8 show that nitrate concentration, open water latent heat flux, wind speed, and chl *a* concentration had an inverse

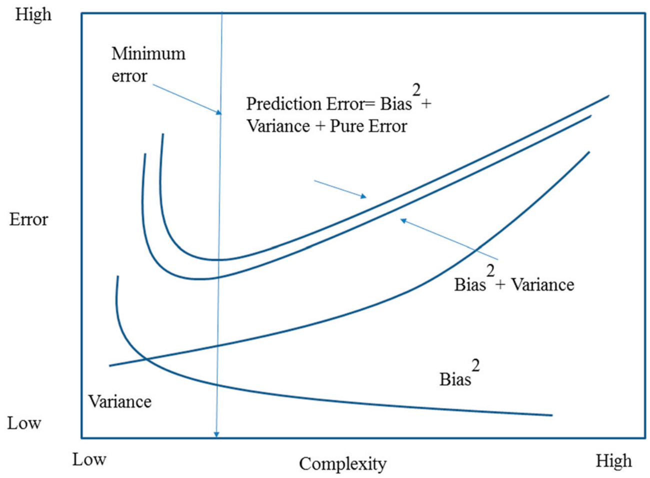

Fig. 5 Trade-off between model complexity, bias, and variance.

relationship with SST, while air temperature and ozone mass mixing ratios were positively correlated with SST. According to Fig. 8, SST drastically increased when the air temperature exceeded 25.85°C (299 K). When the nitrate concentration varied from 0 to 1 µmol L^{-1}, the SST decreased from 28.5°C to 28.1°C. Nitrate concentrations less than 1 µmol L^{-1} correlated strongly with SSTs in this region. When the open water latent energy flux increased from 120–160 W m^{-2}, SST decreased from 28.3°C to 28.1°C. When the average surface wind speed increased from 4 to 8 m s^{-1}, SST decreased from 28.3°C to 28.1°C. When chl *a* concentration increased from 0 to 1 mg m^{-3}, the SST decreased from 28.22°C to 28.14°C. The ozone mass mixing ratio increased from 5.0 to 5.25 when the SST increased from 28.16°C to 28.26°C. The linear relationships between each of the influencing variables and SST are also plotted in Fig. 9, but no significant

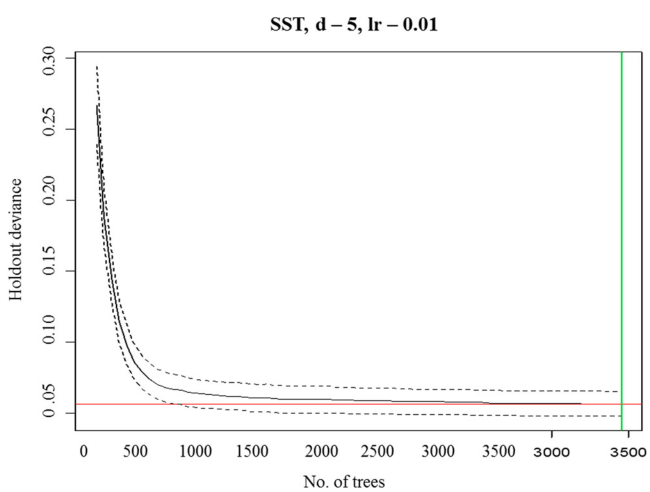

Fig. 6 The relationship between number of trees and holdout deviance for models fitted with five learning rates and two levels of tree complexity. The red line shows the minimum of the mean and the green line the number of trees at which that occurs.

TABLE 2. Relative influence of each environmental variable on SST in the simplified BRT model.

Variable	Relative Influence (%)
Air temperature	47.09837
Nitrate concentration	17.59851
Open water latent energy flux	5.492066
Surface wind speed	4.778454
Chlorophyll *a* concentration	2.577776
Ozone mass mixing ratio	2.226707

relationships were found in others except the positive relationship with air temperature.

4 Discussion

a *Seasonal Changes in Hydro-Climatic Variables in Sri Lankan Waters*

Seasonal maxima and variations for the parameters considered are listed in Table 3. Within the study area, comparatively high wind speeds were observed during the summer monsoonal period. South Asia experiences two monsoons, the southwest, or summer, monsoon from June to September and the northeast, or winter, monsoon from October to December. The summer monsoon is responsible for the majority of the annual rainfall over northern India. During the withdrawal phase of the summer monsoon, lower-level winds over southern Asia reverse direction (i.e., from southwest to northeast), and this is associated with the southward movement of the intertropical convergence zone (ITCZ) and the subtropical anticyclone. The relationship between ENSO and winter monsoon rain over southern Asia is then strengthened because of stronger easterly wind anomalies and anomalously low levels of moisture convergence over the NIO (P. Kumar et al., 2007).

Within the study region, both SST and air temperature are comparatively high during the March to May season, and it is during this time period that the tropics receive the maximum amount of solar radiation for the year (Billings et al., 1981). Moreover, SST in the Indian and Pacific Oceans is influenced by the Australasian monsoon. The warmest region expands during February, March, and April to cover a large portion of the Indian Ocean (20°S–20°N) (Krishnamurthy & Kirtman, 2003). During these months, surface winds are mostly northeasterly in the north and southeasterly in the south, and the surface wind intensifies across the entire Indian Ocean (Krishnamurthy & Kirtman, 2003).

Concentrations of chl *a* within the study area were high from June to September. There is a relationship between chl *a* and eddies in the NIO; the chl *a* concentration is much higher during June, July, and August when anticyclonic eddies occur across the entire basin (Dufois et al., 2014). Mesoscale eddies are also common features of oceanic circulation, which improve primary production by circulating nutrients (Chelton et al., 2011). The West Indian Coastal Current in the AS flows south along the coastlines of western India and Sri Lanka and joins the eastward-flowing Southwest Monsoon Current. The anti-clockwise Lakshadweep eddy

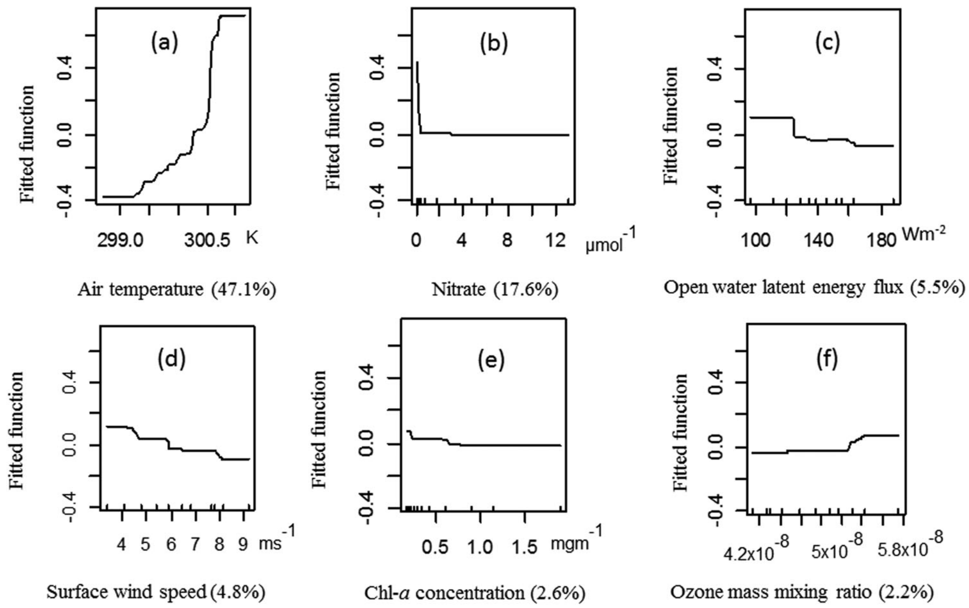

Fig. 7 Fitted relationships from the simplified BRT model for each of the predictor variables (*x*-axis) and the SST (*y*-axis): (a) air temperature, (b) nitrate, (c) open water latent energy flux, (d) wind speed, (e) chl *a* concentration, and (f) ozone mass mixing ratio.

off the southwestern coast of India also modifies the currents in this region (Schott et al., 1994). The Southwest Monsoon Current flows along the southern coast of Sri Lanka from west to east, transporting approximately 848 $m^3\ s^{-1}$ of water between the equator and Sri Lanka (Schott et al., 1994). After passing the coast of Sri Lanka, the currents form a counterclockwise eddy, called the Sri Lanka Dome, which is centred at 7°N, 83°E (Schott et al., 1994).

Within the study region, the changing pattern of chl *a* concentration is similar to the pattern of nitrate variability from June to September. The nitrate levels during these months were relatively stable and optimal. Weakened westerly and easterly wind stress magnitudes also occurred in June and August. This results in equatorial and coastal downwelling Kelvin waves forming along the eastern rim of the BoB, and westward-propagating Rossby waves generate strong

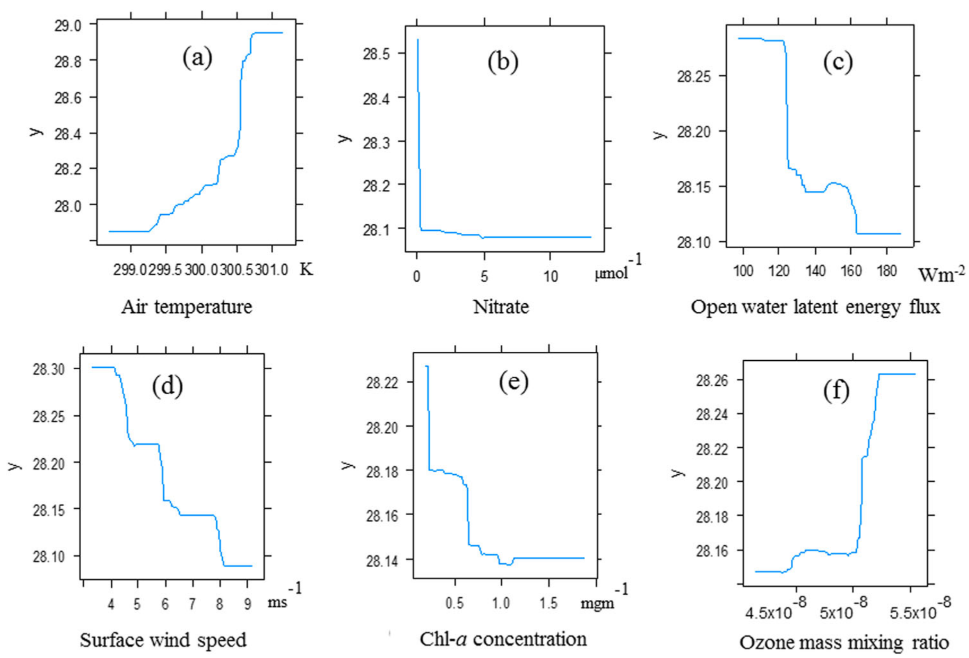

Fig. 8 SST relationships from the simplified BRT model for each of the predictor variables (*x*-axis) and the SST change (*y*-axis): (a) air temperature, (b) nitrate, (c) open water latent energy flux, (d) wind speed, (e) chl *a* concentration, and (f) ozone mass mixing ratio.

anticyclonic eddies (Gulakaram et al., 2018). Eddy-induced Ekman pumping, due to the interaction between eddy surface currents and winds, generates upwelling in the central part of the ocean (Dufois et al., 2014), providing nutrients to the surface waters.

Nitrate concentrations (Fig. 4d) during the September to November season showed considerable fluctuations and were highest in 2005, 2007, and 2009. Some studies have suggested that cyclones influence nitrate concentrations by mixing surface and deep water (Sarangi, 2011). In 2005, Cyclone Baaz formed in the eastern BoB, and Cyclone Fanoos formed in the South Andaman Sea. In 2007, Cyclone Akash formed in the east-central BoB, Super Cyclone Gonu formed in the eastern AS, and Cyclone Yemyin occurred in the BoB. In 2009, Cyclone Bijli formed in the central BoB, Cyclone Phyan formed southwest of Colombo, Sri Lanka, and Cyclone Ward formed southeast of Batticaloa, Sri Lanka. These cyclonic storm systems may have resulted in the high nitrate concentrations observed during these years.

High ozone mass mixing ratios were observed during late spring and early summer (March–May). This likely reflects large-scale photochemical production resulting from the presence of NO_x, carbon monoxide, and hydrocarbon precursors distributed as air masses move over polluted areas (Sonkaew & Macatangay, 2015).

b *BRT Model Performance for SST and Predictor Variables*

Many previous studies have identified SST as a major contributor to climate variations. Because more trees were included in the partial plot in the BRT model of SST, the response to summer temperature became more complex and curvilinear. The results (Figs 7 and 8) suggest that atmospheric, oceanic, and biological components in the NIO are associated with SST variability. Air temperature significantly affects SST and, in this case, showed a positive relationship. When the air temperature rose above 300 K (~27°C), SST increased dramatically. This is in agreement with previous studies. For example, Newell and Wu (1992) showed that a change in air temperature of 0.7°C over the global oceans is associated with a 1°C change in SST. Schneider and Qi (2015) indicated that horizontal advection (horizontal heat transport) via wind, air–sea fluxes, and lateral mixing balance the atmospheric-oceanic heat budget. Schneider and Qiu found that the SST-induced circulation, the order of the heat budget balances horizontal advection by the vertically averaged background winds with the air–sea fluxes and lateral mixing This phenomenon can be represented mathematically by

$$\overline{\mathbf{u}^{(0)}} \cdot \nabla\Theta^{(1)} = \gamma_\Theta[T^{(1)} - \Theta^{(1)}] + A_h\nabla^2\Theta^{(1)}$$

where, $\Theta^{(1)}$ is the frontally induced atmospheric temperatures; $\overline{\mathbf{u}^{(0)}}$ is the background horizontal wind; T is sea surface temperature; γ_Θ is the adjustment rate of SST; A_h is the lateral diffusion coefficient; and $T^{(1)} - \Theta^{(1)}$ is the frontally altered stability.

Open water latent energy fluxes below 130 W m^{-2} were strongly associated with SSTs between 28.15°C and 28.28°C. However, this was a complex non-linear relationship. He et al. (2017) found that a variety of processes contribute to SST tendencies in the Indian Ocean. Some studies have suggested that the negative tendency correlation of the latent heat flux and SST indicates the dominance of atmospheric forcing of the ocean in the mid-latitudes, the dominance of oceanic forcing of the atmosphere in the eastern equatorial Pacific and Atlantic, and the contribution of atmospheric forcing to SST variations in the eastern Indian Ocean and western Pacific Ocean (Wu et al., 2007). Thus, air–sea heat fluxes contribute to the warming of the ocean (Benthuysen et al., 2014) although this relationship varies regionally. Positive latent energy flux and SST correlation are observed in the eastern equatorial Pacific and Atlantic, western North Pacific, western North Atlantic, tropical North Atlantic, the southwest coast of Australia, and the south of Africa, while it is negative in the equatorial central-western Pacific (Wu et al., 2007).

Wind speeds up to 8 m s^{-1} were correlated with SST values above 28.1°C, and these two variables were negatively correlated overall. Shukla and Misra (1977) also observed a negative relationship between SST and wind speed in the AS. Their work indicated that evaporation, enhanced upwelling, and the spread of cold coastal waters occur when winds are strong, resulting in lower SSTs. Consequently, low SST and high wind speeds tended to correlate with higher nutrient (i.e., nitrate) concentrations. Nitrate concentration is also linked to SST and is an indicator of the upwelling associated with warm pool effects (Silió-Calzada et al., 2008). In this study, and previous studies (e.g. Silió-Calzada et al., 2008), it has been shown that nitrate has an inverse relationship with SST; in the study region, nitrate concentrations increased

TABLE 3. Seasonal maximum and variations of the studied variables.

Variable	Peak Season within the Study Period	Year	Highest Value	Units	Highest Months
Surface wind speed	JJA	2004	8.70869446	m s^{-1}	JJA
SST	MAM	2005	29.35702703	°C	MAM
Ozone mass mixing ratio	DJF	2004	5.25727×10^{-8}	kg kg^{-1}	MAM
Nitrate concentration	SON	2009	9.231374273	µmole L^{-1}	SON
Latent heating	SON	2006	0.155569635	W m^{-2}	SON
Chlorophyll *a* concentration	JJA	2004	1.61579	mg m^{-3}	JJA
Air temperature	MAM	2005	300.7259623	K	MAM

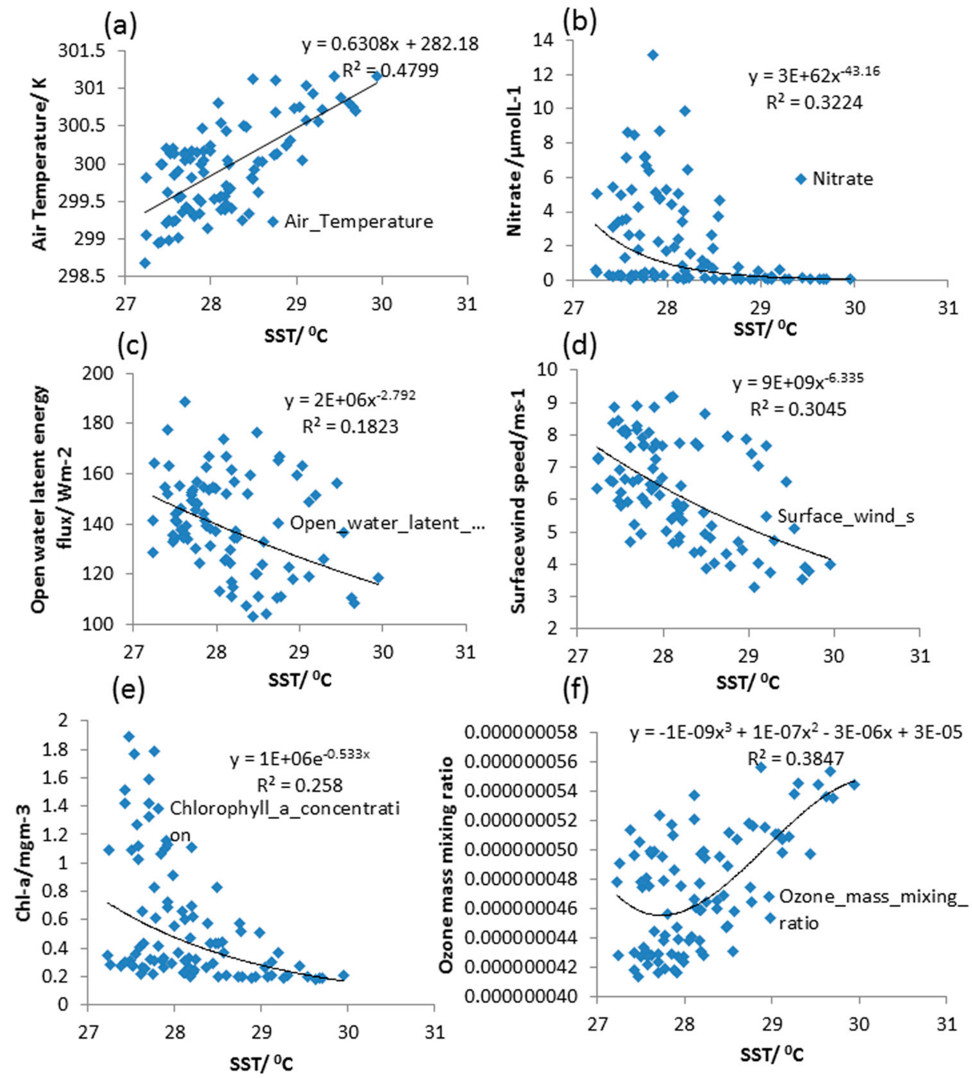

Fig. 9 SST changing trend with the predictor variables *x*-axis – SST; *y*-axis – studied variable. (a) air temperature, (b) nitrate, ~~(C)~~ (c) open water latent energy flux, (d) wind speed, ~~(f)~~ (e) chl *a* concentration, and ~~(g)~~ (f) ozone mass mixing ratio.

from 0 to 0.2 µmol L^{-1} as SSTs decreased from 28.5°C to 28.1°C.

Based on the relationship between SST and chl *a* concentration established by the BRT model, a surface water temperature of approximately 28.14°C was associated with high chl *a* concentrations. The relationships between these two variables have also been observed in previous studies (e.g., Abdellaoui, 2017; Kraemer et al., 2017; G. S. Kumar et al., 2016; Luis & Kawamura, 2004). The results also show that high wind speeds and cold SST promote upwelling, which brings essential nutrients to the surface resulting in phytoplankton blooms. When the sea surface warms, the circulation of nutrients decreases, and surface temperatures become suboptimal for phytoplankton (Grimaud et al., 2015).

The BRT model also revealed a positive correlation between SST and the ozone mass mixing ratio; when the ozone mass mixing ratio increased to greater than 5×10^{-8}, much higher SSTs were observed. Sonkaew and Macatangay (2015) stated that interannual variability in the tropospheric ozone column is modulated by ENSO events, leading to SST anomalies. This SST lag occurs because of the coupled characteristics of the atmosphere–ocean system. The tropospheric ozone column concentration decreases from neutral periods to strong La Niña periods, enhancing precipitation. This enhanced convection produces more thunderstorms, with lightning strikes being associated with tropospheric ozone nitrates (National Research Council, 1991). During El Niño periods, the opposite process may occur. The sensitive balance between these factors causes interannual variability in the tropospheric ozone column (Sonkaew & Macatangay, 2015). Nowack et al. (2017) found that changes in ozone concentrations in the tropical upper troposphere and lower stratosphere driven by CO_2 counteracts the effect of reducing the vertical temperature gradient in the tropical troposphere in climate models, which acts to slow the Walker circulation. The

Walker circulation is closely coupled with ENSO and, therefore, changes in ozone lead to SST gradients and land–sea temperature contrasts that may reduce the amplitude of ENSO events (Nowack et al., 2017).

5 Conclusions

Wind speed and SST act as the major regulating factors of atmospheric and oceanic climate in the NIO. According to the BRT model, nitrate concentration, open water latent heat flux, wind speed, and chl *a* concentration have inverse relationships with SST, while air temperature and ozone mass mixing ratio have positive relationships with SST. The highly correlated ranges in air temperature, nitrate concentration, open water latent energy flux, surface wind speed, chl *a* concentration, and ozone mass mixing ratio for an SST above 28°C were 299–300.5 K, more than 0.2 $\mu mol\ L^{-1}$, 120–160 $W\ m^{-2}$, 4–8 $m\ s^{-1}$, 0.1–1 $mg\ m^{-3}$, and $4.5–5.5 \times 10^{-8}$, respectively. The findings address the overall aim of this study by identifying the relationship between SST and the parameters studied. Another objective fulfilled by this study was identifying the optimum range of SST that specifically affects phytoplankton growth within the study region. This is the first attempt to assess relationships between SST and the variables studied in this region of the world, specifically, using these satellite datasets and modelling approach. It will open up pathways for understanding the climatological influence on the ecosystems in the NIO and for preparing the necessary policies to mitigate the deleterious effects that may occur with the severe scenarios of future climate change. This study will help in developing methods for more precise estimation of the complex nature of SST and ocean subsurface temperature by considering the most effective parameters. Moreover, this study identified a BRT as a suitable modelling method that deals robustly with the non-linear relationships of SST and the other parameters in this region, which will help in modelling and predicting climate variables in this region in the context of on-going climate change.

Acknowledgements

We thank MODIS mission scientists and associated NASA personnel, ERDDAP, and the Indian Ocean Tuna Commission for providing data. We are grateful to Dr. Suranga Kodithuwakku (University of Peradeniya) for the guidance given. We also express our sincere thanks to the reviewers and the editor of the journal.

Disclosure statement

No potential conflict of interest was reported by the author(s).

Funding

This research was funded by the National Natural Sciences Foundation of China [grant number 41430968], [grant number 41876136]; the Collaborative Innovation Center for 21st-Century Maritime Silk Road Studies, Guangzhou, China [grant number 2015HS05]; the China Scholarship Council [grant number 14412016G005]; the Prince Albert II of Monaco Foundation and Guandong Research Funding [grant number 2019BT2H594] and [grant number GML2019ZD0602].

ORCID

Thushani Suleka Madhubhashini Elepathage http://orcid.org/0000-0002-0449-1228

References

Abdellaoui, B. (2017). Assessing the impact of temperature and chlorophyll variations on the fluctuations of sardine abundance in Al-Hoceima (South Alboran Sea). *Journal of Marine Science: Research & Development*, *7* (4), Article 239. https://doi.org/10.4172/2155-9910.1000239

Benthuysen, J., Feng, M., & Zhong, L. (2014). Spatial patterns of warming off western Australia during the 2011 Ningaloo Niño: Quantifying impacts of remote and local forcing. *Continental Shelf Research*, *91*, 232–246. https://doi.org/10.1016/j.csr.2014.09.014

Billings, W. D., Golley, F., Lange, O. L., Olson, J. S., & Remmert, H. (1981). *Ecological studies analysis and synthesis*. (P.C. Miller, Ed., Vol. 39). Springer-Verlag.

Chakrabarthi, A. (2019). Carbon emissions and sea surface temperature: Why cyclonic storms are on the rise in Arabian Sea - News18. *News 18*. https://www.news18.com/news/india/carbon-emissions-and-sea-surface-temperature-why-cyclonic-storms-are-on-the-rise-in-arabian-sea-2186055.html

Chelton, D. B., Schlax, M. G., & Samelson, R. M. (2011). Global observations of nonlinear mesoscale eddies. *Progress in Oceanography*, *91*(2), 167–216. https://doi.org/10.1016/J.POCEAN.2011.01.002

D'Addezio, J. M., Subrahmanyam, B., Nyadjro, E. S., Murty, V. S. N. (2015). Seasonal variability of salinity and salt transport in the northern Indian Ocean. *Journal of Physical Oceanography*, *45*(7), 1947–1966. https://doi.org/10.1175/JPO-D-14-0210.1

De Vos, A., Pattiaratchi, C. B., & Wijeratne, E. M. S. (2014). Surface circulation and upwelling patterns around Sri Lanka. *Biogeosciences*, *11*(20), 5909–5930. https://doi.org/10.5194/bg-11-5909-2014

De'ath, G. (2007). Boosted trees for ecological modeling and prediction. *Ecology*, *88*(1), 243–251. https://doi.org/10.1890/0012-9658(2007)88[243:BTFEMA]2.0.CO;2

Department of Meteorology. (2018). *Climate of Sri Lanka*. http://www.meteo.gov.lk/index.php?option=com_content&view=article&id=94&Itemid=310&lang=en#4-northeast-monsoon-season-december-february

Ding, H., & Elmore, A. J. (2015). Remote sensing of environment spatio-temporal patterns in water surface temperature from Landsat time series data in the Chesapeake Bay, U.S.A. *Remote Sensing of Environment*, *168*, 335–348. https://doi.org/10.1016/j.rse.2015.07.009

Dorji, P., & Fearns, P. (2017). Impact of the spatial resolution of satellite remote sensing sensors in the quantification of total suspended sediment concentration : A case study in turbid waters of northern western Australia. *PLOS ONE*, *12*(4), 1–24. https://doi.org/10.1371/journal.pone.0175042

Dufois, F., Hardman-Mountford, N. J., Greenwood, J., Richardson, A. J., Feng, M., Herbette, S., & Matear, R. (2014). Impact of eddies on surface chlorophyll in the south Indian Ocean. *Journal of Geophysical Research: Oceans*, *119*(11), 8061–8077. https://doi.org/10.1002/2014JC010164

Elith, J., & Leathwick, J. (2017). Boosted regression trees for ecological modeling. https://cran.r-project.org/web/packages/dismo/vignettes/brt.pdf

Elith, J., Leathwick, J. R., & Hastie, T. (2008). A working guide to boosted regression trees. *Journal of Animal Ecology*, *77*(4), 802–813. https://doi.org/10.1111/j.1365-2656.2008.01390.x

Govil, P., & Naidu, P. D. (2011). Variations of Indian monsoon precipitation during the last 32kyr reflected in the surface hydrography of the western Bay of Bengal. *Quaternary Science Reviews*, *30*(27–28), 3871–3879. https://doi.org/10.1016/j.quascirev.2011.10.004

Grimaud, G. M., Le Guennec, V., Ayata, S.-D., Mairet, F., Sciandra, A., & Bernard, O. (2015). Modelling the effect of temperature on phytoplankton growth across the global Ocean. *IFAC-PapersOnLine*, *48*(1), 228–233. https://doi.org/10.1016/J.IFACOL.2015.05.059

Gulakaram, V. S., Vissa, N. K., & Bhaskaran, P. K. (2018). Role of mesoscale eddies on atmospheric convection during summer monsoon season over the Bay of Bengal: A case study. *Journal of Ocean Engineering and Science*, *3*(4), 343–354. https://doi.org/10.1016/J.JOES.2018.11.002

Hansen, J., Sato, M., & Ruedy, R. (1997). Radiative forcing and climate response. *Journal of Geophysical Research: Atmospheres*, *102*(D6), 6831–6864. https://doi.org/10.1029/96JD03436

He, Z., Wu, R., Wang, W., Wen, Z., Wang, D., He, Z., Wu, R., Wang, W., Wen, Z., & Wang, D. (2017). Contributions of surface heat fluxes and oceanic processes to tropical SST changes: Seasonal and regional dependence. *Journal of Climate*, *30*(11), 4185–4205. https://doi.org/10.1175/JCLI-D-16-0500.1

Hood, R., Naqvi, W., Wiggert, J., Goes, J., Coles, V., McCreary, J., Bates, N., Karuppasamy, P. K., Mahowald, N., Seitzinger, S., & Meyers, G. (2008). Research opportunities and challenges in the Indian Ocean. *Eos, Transactions American Geophysical Union*, *89*(13), 125–126. https://doi.org/10.1029/2008EO130001

Humaira, R. A., Miftahuddin, & Setiawan, I. (2019). Modelling of sea surface temperature by using generalized additive mixed models in risk detection. *IOP Conference Series: Earth and Environmental Science*, *273*, Article 012025. https://doi.org/10.1088/1755-1315/273/1/012025

Izumo, T., Montégut, C. B., Luo, J.-J., Behera, S. K., Masson, S., Yamagata, T., & Izumo, T. (2008). The role of the western Arabian Sea upwelling in Indian monsoon rainfall variability. *Journal of Climate*, *21*(21), 5603–5623. https://doi.org/10.1175/2008JCLI2158.1

Jensen, T. G. (2001). Arabian Sea and Bay of Bengal exchange of salt and tracers in an ocean model. *Geophysical Research Letters*, *28*(20), 3967–3970. https://doi.org/10.1029/2001GL013422

Kamykowski, D. (1987). A preliminary biophysical model of the relationship between temperature and plant nutrients in the upper ocean. *Deep-Sea Research*, *34*(7), 1067–1079. https://doi.org/10.1016/0198-0149(87)90064-1

Karagali, I., Høyer, J., & Hasager, C. (2012). Remote sensing of environment SST diurnal variability in the North Sea and the Baltic Sea. *Remote Sensing of Environment*, *121*, 159–170. https://doi.org/10.1016/j.rse.2012.01.016

Kay, S., Caesar, J., & Janes, T. (2018). *Marine dynamics and productivity in the Bay of Bengal. Ecosystem services for well-being in deltas*. Springer International. https://doi.org/10.1007/978-3-319-71093-8_14

Khole, M. (2003). Variability of sea surface temperature over Indian Ocean during El-Nino and La-Nina years. *MAUSAM: Quarterly Journal of* ~~*meteorology,*~~ *Hydrology & Geophysics*, *54*(4), 829–836.

Kraemer, B. M., Mehner, T., & Adrian, R. (2017). Reconciling the opposing effects of warming on phytoplankton biomass in 188 large lakes. *Scientific Reports*, *7*(1), 10762. https://doi.org/10.1038/s41598-017-11167-3

Krishnamurthy, V., & Kirtman, B. P. (2003). Variability of the Indian Ocean: Relation to monsoon and ENSO. *Quarterly Journal of the Royal Meteorological Society*, *129*, 1623–1646. https://doi.org/10.1256/qj.01.166

Kumar, A., & Hoerling, M. P. (2003). The nature and causes for the delayed atmospheric response to El Niño. *Journal of Climate*, *16*(9), 1391–1403. https://doi.org/10.1175/1520-0442-16.9.1391

Kumar, G. S., Prakash, S., Ravichandran, M., & Narayana, A. C. (2016). Trends and relationship between chlorophyll-a and sea surface temperature in the central equatorial Indian Ocean. *Remote Sensing Letters*, *7*(11), 1093–1101. https://doi.org/10.1080/2150704X.2016.1210835

Kumar, O. B., Naidu, C. V., & Rao, S. R. L. (2004). Influence of southern oscillation and SSTs over Nino-3.4 region on the winter monsoon rainfall over coastal Andhra Pradesh. *Proceedings of the Indian Academy of Sciences (Earth & Planetary Sciences)*, *113*(3), 313–319. ~~https://doi.org/10.1007/s00382-006-0210-0~~

Kumar, P., Rupa Kumar, K., Rajeevan, M., & Sahai, A. K. (2007). On the recent strengthening of the relationship between ENSO and northeast monsoon rainfall over south Asia. *Climate Dynamics*, *28*(6), 649–660. https://doi.org/10.1007/s00382-006-0210-0

Kumar, P. S., Pillai, G. N., & Manjusha, U. (2014). El Nino Southern Oscillation (ENSO) impact on tuna fisheries in Indian Ocean. *Springer Plus*, *3*(591), 1–13. https://doi.org/10.1186/2193-1801-3-591

Kumar, S. P., Roshin, R. P., Narvekar, J., Dinesh Kumar, P. K., & Vivekanandan, E. (2009). Response of the Arabian Sea to global warming and associated regional climate shift. *Marine Environmental Research*, *68*(5), 217–222. https://doi.org/10.1016/J.MARENVRES.2009.06.010

Lau, N.-C., Leetmaa, A., Nath, M. J., Wang, H.-L., Lau, N.-C., Leetmaa, A., Nath, M. J., & Wang, H.-L. (2005). Influences of ENSO-induced Indo–western Pacific SST anomalies on extratropical atmospheric variability during the boreal summer. *Journal of Climate*, *18*(15), 2922–2942. https://doi.org/10.1175/JCLI3445.1

Lee, C. M., Jones, B. H., Brink, K. H., & Fischer, A. S. (2000). The upper-ocean response to monsoonal forcing in the Arabian Sea: Seasonal and spatial variability. *Deep Sea Research Part II: Topical Studies in Oceanography*, *47*(7–8), 1177–1226. https://doi.org/10.1016/S0967-0645(99)00141-1

Lévy, M., Shankar, D., André, J.-M., Shenoi, S. S. C., Durand, F., & de Boyer Montégut, C. (2007). Basin-wide seasonal evolution of the Indian Ocean's phytoplankton blooms. *Journal of Geophysical Research*, *112*(C12), C12014. https://doi.org/10.1029/2007JC004090

Luis, A. J., & Kawamura, H. (2004). Air-sea interaction, coastal circulation and primary production in the eastern Arabian Sea: A review. *Journal of Oceanography*, *60*(2), 205–218. https://doi.org/10.1023/B:JOCE.0000038327.33559.34

Madhubhashini, E. T. S., Tang, D., & Oey, L. (2019). The Pelagic habitat of Swordfish (*Xiphias gladius*) in the changing environment of the North Indian Ocean. *Sustainability*, *11*(24), Article 7070. https://doi.org/10.3390/su11247070

Murtugudde, R., Seager, R., & Thoppil, P. (2007). Arabian Sea response to monsoon variations. *Paleoceanography*, *22*, ~~A~~A4217. https://doi.org/10.1029/2007PA001467

Nandkeolyar, N., Raman, M., & Sandhya Kiran, G. (2013). Comparative analysis of sea surface temperature pattern in the eastern and western gulfs of Arabian Sea and the Red Sea in recent past using satellite data. *International Journal of Oceanography*, *2013*, Article 501602. https://doi.org/10.1155/2013/501602

Narvekar, J., & Prasanna Kumar, S. (2014). Mixed layer variability and chlorophyll a biomass in the Bay of Bengal. *Biogeosciences*, *11*, 3819–3843. https://doi.org/10.5194/bg-11-3819-2014

NASA. (2016). EarthData: Giovanni: The bridge between data and science v 4.33. https://giovanni.gsfc.nasa.gov/giovanni/

National Research Council. (1991). *The effects of meteorology on tropospheric ozone. Rethinking the ozone problem in urban and regional air pollution*. The National Academies Press. https://www.nap.edu/read/1889/chapter/6#95

Newell, R. E., & Wu, Z.-X. (1992). The interrelationship between temperature changes in the free atmosphere and sea surface temperature changes. *Journal of Geophysical Research*, *97*(D4), 3693–3709. https://doi.org/10.1029/91JD03079

Nowack, P. J., Braesicke, P., Luke Abraham, N., & Pyle, J. A. (2017). On the role of ozone feedback in the ENSO amplitude response under global warming. *Geophysical Research Letters*, *44*(8), 3858–3866. https://doi.org/10.1002/2016GL072418

Oke, P. R., Larnicol, G., Fujii, Y., Smith, G. C., Lea, D. J., Guinehut, S., Remy, E., Alonso Balmaseda, M., Rykova, T., Surcel-Colan, D., Martin, M. J., Sellar, A. A., Mulet, S., & Turpin, V. (2015). Assessing the impact of observations on ocean forecasts and reanalyses: Part 1, global studies. *Journal of Operational Oceanography*, *8*, s49–s62. https://doi.org/10.1080/1755876X.2015.1022067

Qasim, S. Z. (1982). Oceanography of the northern Arabian Sea. *Deep Sea Research Part A. Oceanographic Research Papers*, *29*(9), 1041–1068. https://doi.org/10.1016/0198-0149(82)90027-9

Roxy, M., Tanimoto, Y., Preethi, B., Terray, P., & Krishnan, R. (2013). Intraseasonal SST-precipitation relationship and its spatial variability over the tropical summer monsoon region. *Climate Dynamics*, *41*(1), 45–61. https://doi.org/10.1007/s00382-012-1547-1

Sarangi, R. K. (2011). Remote-sensing-based estimation of surface nitrate and its variability in the southern peninsular Indian waters. *International Journal of Oceanography*, *2011*(January), 1–16. https://doi.org/10.1155/2011/172731

Sarangi, R. K., & Nanthini Devi, K. (2017). Space-based observation of chlorophyll, sea surface temperature, nitrate, and sea surface height anomaly over the Bay of Bengal and Arabian Sea. *Advances in Space Research*, *59*(1), 33–44. https://doi.org/10.1016/j.asr.2016.08.038

Sarma, V. V. S. S., Lenton, A., Law, R. M., Metzl, N., Patra, P. K., Doney, S., Lima, I. D., Dlugokencky, E., Ramonet, M., & Valsala, V. (2013). Sea-air CO_2 fluxes in the Indian Ocean between 1990 and 2009. *Biogeosciences*, *10*, 7035–7052. https://doi.org/10.5194/bg-10-7035-2013

Sarmiento, J. L., Wofsy, S. C., Shea, E., Scott Denning, A., Easterling, W., Field, C., Fung, I., Keeling, R., McCarthy, J., Pacala, S., Post Oak, W. M., Schimel, D., Sundquist, E., Tans, P., Weiss, R., & Yoder, J. (1999). *A U.S. carbon cycle science plan - carbon and climate working group (U.S.) - Google Books*. U.S. Global Change Research Program. https://jacksonlab.stanford.edu/publication/us-carbon-cycle-science-plan-us-carbon-cycle-science-program-washington-dc

Schneider, N., & Qiu, B. (2015). The atmospheric response to weak sea surface temperature fronts. *Journal of the Atmospheric Sciences*, *72*(9), 3356–3377. https://doi.org/10.1175/JAS-D-14-0212.1

Schott, F., Reppin, J., Fischer, J., & Quadfasel, D. (1994). Currents and transports of the monsoon current south of Sri Lanka. *Journal of Geophysical Research*, *99*(C12), 25127–25141. https://doi.org/10.1029/94JC02216

Sengupta, D., Senan, R., Goswami, B. N., & Vialard, J. (2007). Intraseasonal variability of equatorial Indian Ocean zonal currents. *Journal of Climate*, *20*, 3036–3055. https://doi.org/10.1175/JCLI4166.1

Shamsad, M., Farukh, M. A., Chowdhury, M. J. R., & Basak, S. C. (2013). Sea surface temperature anomaly in the Bay of Bengal in 2010. *Journal of Environmental Science and Natural Resources*, *5*(2), 77–80. https://doi.org/10.3329/jesnr.v5i2.14797

Shankar, D., Vinayachandran, P. N., & Unnikrishnan, A. S. (2002). The monsoon currents in the North Indian Ocean. *Progress in Oceanography*, *52*(1), 63–120. https://doi.org/10.1016/S0079-6611(02)00024-1

Sharma, D. C. (2017). Warming of Arabian Sea is causing extreme rainfall events: Study. *The Hindu Business Line*. https://www.thehindubusinessline.com/news/science/warming-of-arabian-sea-is-causing-extreme-rainfall-events-study/article9887200.ece

Shono, H. (2001). Comparison of statistical models for CPUE standardization by information criteria Poisson model vs. log-normal model. *IOTC Proceedings*, *4*(4), 219–224. https://iotc.org/documents/comparision-statistical-models-cpue-standardisation-information-criteria-poisson-model-vs

Shukla, J. (1998). Predictability in the midst of chaos: A scientific basis for climate forecasting. *Science (New York, N.Y.)*, *282*(5389), 728–731. https://doi.org/10.1126/SCIENCE.282.5389.728

Shukla, J., & Misra, B. M. (1977). Relationships between sea surface temperature and wind speed over the central Arabian Sea, and monsoon rainfall over India. *Monthly Weather Review*, *105*(8), 998–1002. https://doi.org/10.1175/1520-0493(1977)105<0998:RBSSTA>2.0.CO;2

Silió-Calzada, A., Bricaud, A., & Gentili, B. (2008). Estimates of sea surface nitrate concentrations from sea surface temperature and chlorophyll concentration in upwelling areas: A case study for the Benguela system. *Remote Sensing of Environment*, *112*(6), 3173–3180. https://doi.org/10.1016/j.rse.2008.03.014

Sonkaew, T., & Macatangay, R. (2015). Determining relationships and mechanisms between tropospheric ozone column concentrations and tropical biomass burning in Thailand and its surrounding regions. *Environmental Research Letters*, *10*, 065009. https://doi.org/10.1088/1748-9326/10/6/065009

Sumesh, K. G., & Ramesh Kumar, M. R. (2013). Tropical cyclones over North Indian Ocean during El-Niño Modoki years. *Natural Hazards*, *68*(2), 1057–1074. https://doi.org/10.1007/s11069-013-0679-x

Swan, B., & National Museum of Sri Lanka (1983). *An introduction to the coastal geomorphology of Sri Lanka*. National Museums of Sri Lanka. https://trove.nla.gov.au/work/17776438

Tang, D., & Pan, B. (2011). *Remote sensing of the changing oceans*. Springer. https://www.springer.com/gp/book/9783642165405

Tomczak, M. (1988). Island wakes in deep and shallow water. *Journal of Geophysical Research*, *93*(8), 5153–5154. https://doi.org/10.1029/JC093iC05p05153

Trenberth, K. E., Branstator, G. W., Karoly, D., Kumar, A., Lau, N.-C., & Ropelewski, C. (1998). Progress during TOGA in understanding and modeling global teleconnections associated with tropical sea surface temperatures. *Journal of Geophysical Research: Oceans*, *103*(C7), 14291–14324. https://doi.org/10.1029/97JC01444

Vinayachandran, P. N., Chauhan, P., Mohan, M., & Nayak, S. (2004). Biological response of the sea around Sri Lanka to summer monsoon. *Geophysical Research Letters*, *31*(1), L01302. https://doi.org/10.1029/2003GL018533

Wiggert, J. D., Hood, R. R., Banse, K., & Kindle, J. C. (2005). Monsoon-driven biogeochemical processes in the Arabian Sea. *Progress in Oceanography*, *65*(2–4), 176–213. https://doi.org/10.1016/J.POCEAN.2005.03.008

Wu, R., Kirtman, B. P., & Pegion, K. (2007). Surface latent heat flux and its relationship with sea surface temperature in the national centers for environmental prediction climate forecast system simulations and retrospective forecasts. *Geophysical Research Letters*, *34*(17), L17712. https://doi.org/10.1029/2007GL030751

Yapa, K. K. A. S. (2009). Upwelling phenomena in the southern coastal waters of Sri Lanka during southwest monsoon period as seen from MODIS. *Sri Lankan Journal of Physics*, *10*, 7–15. https://doi.org/10.4038/sljp.v10i0.3831